# A model of gas mixing into single-entrance tree cavities during wildland fires

**A.S. Bova, G. Bohrer, and M.B. Dickinson**

**Abstract:** The level of protection to fauna provided by tree cavities during wildland fires is not well understood. Here we present a model for estimating the transport of combustion gases into cylindrical, single-entrance cavities during exposures caused by different wildland fire scenarios. In these shelters, the entrance occurs near the top of the cavity. This empirical model was developed from a suite of numerical experiments using the National Institute of Standards and Technology's Fire Dynamics Simulator, which spanned a range of entrance diameters, wind speeds, gas temperatures, and vertical angles of incidence. To evaluate the model's predictions, it was used to replicate, with great accuracy, a time series of carbon monoxide (CO) concentrations in a controlled experiment where a fabricated cylindrical cavity was exposed to combustion products. The time constant for cavity filling is proportional to the ratio of cavity volume to entrance area. Hot gases lead to significant stratification within the cavity during exposures. To demonstrate the model's potential use in predicting faunal exposures in the context of land management, we show that the model can be used to estimate dosage within red-cockaded woodpecker (*Picoides borealis* Vieillot, 1809) cavities without requiring temporally detailed, local measurements of wind speed and combustion product concentrations.

**Résumé :** Le degré de protection que procurent les cavités d'arbre pour la faune durant les feux de forêt n'est pas bien connu. Nous présentons ici un modèle pour l'estimation du déplacement des gaz de combustion dans des cavités cylindriques à une seule entrée lors d'expositions correspondant à différents scénarios de feux de forêt. Dans ces abris, l'entrée se trouve près du haut de la cavité. Ce modèle empirique a été développé à partir d'une série d'expériences numériques réalisées à l'aide du simulateur de dynamique du feu du National Institute of Standards and Technology, qui permet de tester une gamme de diamètres d'entrée, de vitesses du vent, de températures des gaz et d'angles verticaux d'incidence. Pour évaluer les prédictions du modèle, le simulateur a été utilisé pour répéter, avec une grande exactitude, une série temporelle de concentrations de monoxyde de carbone (CO) dans une expérience en conditions contrôlées qui consistait à exposer une cavité cylindrique usinée à des produits de combustion. La constante de temps pour le remplissage de la cavité est proportionnelle au ratio du volume de la cavité sur l'aire de l'entrée. Les gaz chauds provoquent une importante stratification dans la cavité durant l'exposition. Pour démontrer la possibilité d'utiliser le modèle pour prédire les expositions de la faune dans un contexte d'aménagement du territoire, nous montrons que le modèle peut être utilisé pour estimer les doses dans des cavités de pic à face blanche (*Picoides borealis* Vieillot, 1809) et ce, sans faire appel à des mesures détaillées dans le temps, à des mesures de vitesse locale du vent ou à des concentrations de produits de combustion.

[Traduit par la Rédaction]

## Introduction

The level of protection afforded by animal shelters such as burrows, tree cavities, and caves during wildland fire events is of interest to wildland fire practitioners and wildlife managers, particularly when endangered or threatened species are involved (e.g., Guelta and Balbach 2005; O'Brien et al. 2006; Engstrom 2010). Fire practitioners need to estimate the impacts of fire use and suppression, and wildlife managers need to assess the adequacy of the shelter resource and sometimes need guidance on how to supplement the resource with artificial shelters. Considerable efforts are made to supplement naturally occurring cavities for a range of mammal and bird species in fire-prone habitats (e.g., Franzreb 1997; Lindenmayer et al. 2009). Although some studies of the mixing of combustion products, or smoke surrogates, into animal shelters have been performed (e.g., Guelta and Checkai 2001; Ar et al. 2004; O'Brien et al. 2006), they did not result in formulas or models that will allow forest and fire managers to easily estimate the probable effects of wildland fires on conditions within such shelters.

A limited number of empirical formulas are available for estimating ventilation rates in natural animal shelters. For example, Okubo and Levin (2001, p. 95) provide a simple formula for the volume flux of air, as a function of wind speed, through prairie dog (*Cynomys ludovicianus*) burrows. However, it is not clear that such relationships will hold for tree

Received 19 October 2010. Accepted 21 April 2011. Published at www.nrcresearchpress.com/cjfr on xx August 2011.

**A.S. Bova and M.B. Dickinson.** USDA Forest Service, 359 Main Road, Delaware, OH 43015, USA.
**G. Bohrer.** College of Civil and Environmental Engineering and Geodetic Science, The Ohio State University, 2070 Neil Ave, Columbus, OH 43210, USA.

**Corresponding author:** M.B. Dickinson (e-mail: mbdickinson@fs.fed.us).

**Table 1.** List of mathematical symbols.

| Symbol | Variable or coefficient | Units |
|---|---|---|
| $A$ | Cavity entrance aperture area | $m^2$ |
| $a$ | Amplitude in empirical curve (Barnett 2002) | unitless |
| AOI | Vertical angle of attack for air approaching the cavity entrance | degrees |
| $c$ | Mass fraction of a substance C, inside the cavity | $kg_C/kg_{air}$ |
| $c_\infty$ | Mass fraction of a substance C, outside the cavity | $kg_C/kg_{air}$ |
| $c_1$ | Mass fraction of a substance C, inside the cavity at time $t = 1$ | $kg_C/kg_{air}$ |
| $c_2$ | Mass fraction of a substance C, inside the cavity at time $t = 2$ | $kg_C/kg_{air}$ |
| $f(\ )$ | Generalized function | unitless |
| $f$(AOI) | AOI normalization factor, to account for the different effects of AOI on e-folding length relative to AOI = 0 | unitless |
| $h$ | Measurement height (aboveground) for wind speed | m |
| $k$ | Proportionality coefficient between e-folding time and the inverse of wind speed | m |
| $k'$ | Linear proportionality coefficient mass flow rate and the ratio of aperture area to wind speed (eq. 1) | unitless |
| $n$ | Statistical sample size | unitless |
| $Q$ | Volume flux | $m^3/s$ |
| $R^2$ | Statistical coefficient of determination of the goodness of fit for a linear regression | unitless |
| $s$ | Shape coefficient in empirical curve relating time from ignition to product concentration (Barnett 2002) | unitless |
| $t$ | Time | s |
| $t_{max}$ | Time of maximum temperature | s |
| $U$ | Wind speed | m/s |
| $\Delta t$ | A time interval, the difference between two arbitrary times $t = 1$ and $t = 2$ | s |
| $\tau$ | e-folding time, the scaling coefficient of the exponential term | s |
| $\rho$ | Air density | $kg/m^3$ |
| $\varphi$ | Mass fraction of an arbitrary ignition product | $kg_C/kg_{air}$ |

cavities exposed to wildland fire plumes, where convective upwelling and increased turbulence will change the flow structure near a cavity.

Gas transport rates into single-entrance structures are especially difficult to estimate. Unlike the above example of ventilation by streaming flow through prairie dog burrows, ventilation induced by external flow around single-entry structures is achieved chiefly by penetration of turbulent eddies through the entrance (Etheridge 2002) and the difference between fluctuating internal and external pressures (Chaplin et al. 2000). This mixing process makes it extremely difficult to estimate, from first principles, the effects of factors such as entry geometry and surrounding turbulence on transport rates into single-entry cavities. Therefore, these relations must be derived empirically from laboratory and field experiments or estimated from numerical simulations.

In this manuscript, we will derive a generalized formulation to predict the concentration of potentially hazardous combustion products inside single-entrance tree cavities. We also describe a suite of experiments to parameterize this method so that it will be practical and could be used to help land managers minimize the impact of prescribed fires on fauna sheltered in these kinds of cavities.

Field experiments covering a range of fire intensities and shelter configurations necessary for a general model of combustion product transport would be costly and probably require many years to complete. Numerical modeling of the interaction between fire and atmosphere and its resulting effects on various animal shelters may, at least in part, fill the near-term need for useful data. We used data from a series of "virtual experiments" to derive a formula for the transport of neutrally buoyant gases into a single-entrance tree cavity. The experiments were performed using the National Institute of Standards and Technology's (NIST) Fire Dynamics Simulator (FDS). FDS's fire-modeling capabilities have been extensively verified and validated (McGrattan et al. 2009*a*), making it a suitable choice for simulating the transport of smoke and hot gases into animal shelters. The derived model was used to accurately replicate measured carbon monoxide (CO) levels in a cylindrical, single-entrance cavity exposed to combustion products during a real-world physical validation experiment.

## Theory

For clarity, all symbols and variables that we use throughout this manuscript are listed in Table 1.

The simplest relationship, a linear relationship for the volume flow ($Q$) in relation to an external wind speed ($U$) through a single window opening of aperture area ($A$), is given by Etheridge (2002) as

$$[1] \qquad Q = k'AU$$

where $k'$ is a linear proportionality coefficient. However, Etheridge (2002) noted that $k'$ is a function of the wind

speed, where the wind speed was measured, the configuration of the entrance, and the structure's overall flow field. Thus, the coefficient in this apparently simple and linear relationship contains hidden, and perhaps nonlinear, complexity. The level of complexity will no doubt be exacerbated for cases affected by the quickly varying wind and temperature fields found in wildland fires.

Assuming that an ideal gas with an inward volumetric flow $Q$ ($m^3 \cdot s^{-1}$) containing a substance at concentration $c_\infty$ mixes instantly into a volume $V$ ($m^3$), the rate of change of concentration $c$ in the volume is given by

$$[2] \qquad \frac{dc}{dt} = \frac{Q}{V}(c_\infty - c)$$

Separating variables and integrating from concentration $c_1$ to $c_2$ over a time interval $\Delta t$ gives

$$[3] \qquad c_2 = c_1 \exp\left(-\frac{\Delta t}{V/Q}\right) + c_\infty \left[1 - \exp\left(-\frac{\Delta t}{V/Q}\right)\right]$$

Adding and subtracting $c_1$ from the right-hand side of eq. 3 and gathering terms gives the following somewhat simplified form:

$$c_2 = (c_\infty - c_1)\left[1 - \exp\left(-\frac{Q}{V}\Delta t\right)\right] + c_1$$

This equation can be used to fit a measurement of concentrations at an arbitrary time, $c_2$, based on the concentration at an earlier time, $c_1$, as a function of the time interval, $\Delta t$. When a time series is available for the empirical fitting, it is possible to determine the exponential scaling time, $V/Q$, that divides $\Delta t$ in eq. 3. We define this time as $\tau \equiv V/Q$. Coefficients that define the scaling of an exponential term are called e-folding coefficients. In eq. 3, this coefficient has the units of seconds and, therefore, $\tau$ is an e-folding time. Note that, by eq. 1, e-folding time may be rewritten as

$$[4] \qquad \tau \equiv \frac{V}{Q} = \frac{k}{u}$$

where the coefficient $k$ (m) is $V/(k'A)$.

Substituting $\tau$ into eq. 3 gives

$$[5] \qquad c_2 = (c_\infty - c_1)\left[1 - \exp\left(-\frac{\Delta t}{\tau}\right)\right] + c_1$$

This equation provides a direct method of predicting the concentration of an arbitrary ignition product inside a cavity, provided that the single coefficient in this equation, the e-folding time $\tau$, can be estimated. However, in single-entrance ventilation and especially in the case of a gases moving through a tunnel connected to a cavity, mixing into the cavity volume will often be far from ideal, as gases entering the tunnel will mix with gases exiting before the cavity is even reached. In addition, flow speeds are often drastically reduced in the tunnel and through the volume, therefore mixing is slow. With this in mind, we expect that, in general, $\tau$ will be proportional to the volume–aperture ratio and inversely proportional to wind speed. We used a combination of physical and virtual experiments to evaluate the e-folding time and provide a generalized formulation with which it could be approximated and used to forecast the concentration of ignition products inside single-entrance cavities of a kind used by many faunal species.

## Methods

### NIST's Fire Dynamics Simulator

FDS is a computational fluid dynamics model designed to simulate thermally driven, low-Mach-number flows (i.e., gas velocities less than 30% of the speed of sound) in various fire scenarios. It solves a modified form of the Navier–Stokes equations using a predictor–corrector algorithm that is second-order accurate (McGrattan et al. 2009*b*). For simulations involving fire, fluid flow solutions are coupled with a mixture fraction combustion model and a radiative transport solver. FDS is actively maintained and updated by NIST developers in close partnership with the user community via online discussion groups and issue tracking (http://fire.nist.gov/fds/).

Turbulence in FDS is usually modeled via large eddy simulation (LES), although direct numerical simulations (DNS) may also be performed in fine-mesh applications. In LES, the movement of the air at scales greater than the mesh cell size is explicitly resolved, and the small cell size guarantees that some of this movement is due to larger turbulent eddies, whereas the effects of turbulence at the smaller, subgrid scales are parameterized.

### Numerical experiments: gas transport into a cylindrical, single-entrance cavity

All cylindrical cavity simulations were performed in a domain of 64 × 64 × 40 cubic cells with 1 cm resolution. FDS requires that the mesh, or numerical grid, in the modeled domain be rectilinear. Virtual objects within a simulation domain are made to conform to the mesh (i.e., a grid cell is either filled by a part of an object or not), thus curved surfaces such as tree boles must be approximated by stepped objects. All exterior boundaries of the domain were "open," that is, all flow crossing the exterior boundaries simply exits the domain. A solid cylinder 30 cm in diameter contained an inner cylindrical cavity of volume 2.58 L, though an additional smaller volume of 2.02 L was used in a separate subset of simulations described below. A 9 cm long tunnel connected the inner cavity to the outside of the solid cylinder. Tunnel diameter was one of the variables in the numerical experiments and ranged from 4 to 10 cm over different trials. In all simulations, the left-side exterior boundary acted as an inlet for a neutrally buoyant tracer gas (molecular mass = 28.9 $g \cdot mol^{-1}$) at a concentration of 1 kg/kg. The mean volumetric concentration of tracer gas within the cavity was recorded at 0.1 s intervals. Inward and outward total gas volume (air and tracer) flux through the entrance tunnel plane, as well as temperatures and wind speeds at the entrance and within the cylinder, were recorded. Although the vertical angles of incidence (AOI), defined here as the vertical angle between the horizontal normal of the entrance plane and the flow (Fig. 1), varied in some cases, the mean horizontal component of flow was always normal to the cylinder entrance plane.

Three simulation suites were implemented using the 2.58 L cylinder. In the first, gas temperature and AOI remained constant at 20 °C and 0°, respectively, while inlet

**Fig. 1.** Schematic diagram of the single-entrance cavity experiment. The left-hand box illustrates the design of the cavity, and the diagram on the right shows the field experiment configuration. Gas enters the domain at an angle of attack (AOA). For example, the flow direction corresponding with an AOA = 45° from horizontal is illustrated by the solid arrow; the centerline perpendicular to the entrance plane (AOI = 0°) is indicated by a broken line.

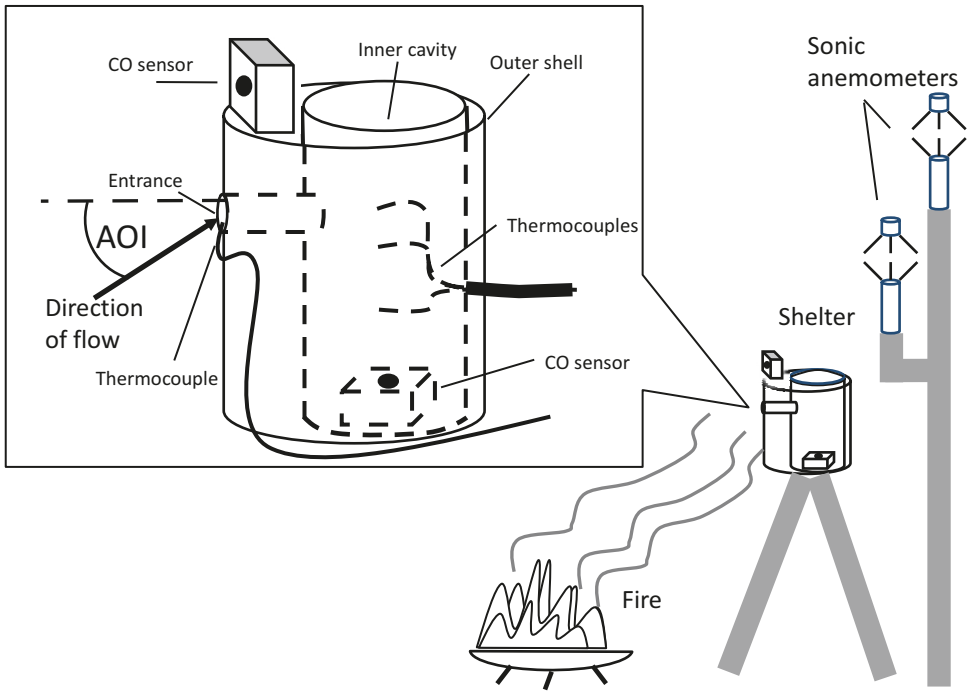


wind speeds increased continuously and linearly through a range of 0 to 5 m·s$^{-1}$ over 50 s of simulated time and then remained constant at 5 m·s$^{-1}$ for an additional 5 s. A subset of simulations, comprising these same boundary conditions, was also carried out for a cylinder with a smaller inner volume of 2.02 L. In the second suite, inlet wind speed and AOI were constant at 1.5 m·s$^{-1}$ and 0°, respectively, but inlet gas temperature increased linearly through a range of 20 to 220 °C over the course of 55 s of simulated time and then remained constant to the end of the simulation (60 s). In the final suite, inlet wind speed and temperature were constant at 2 m·s$^{-1}$ and 20 °C, respectively, while one of five AOI (0°, 30°, 45°, 60°, 90°) were imposed at the inlet. Entrance diameters were 5, 6, 7, 8, 9, and 10 cm in the separate simulations comprising the first two suites, whereas diameters of 5, 7, and 9 cm were used in the final suite (Table 2). The entrance diameters and volumes used in the virtual experiments are within the ranges characteristic of several species of cavity-nesting birds in North America (Aubrey and Raley 2002). Because of the rectilinear mesh, the entrances were not perfectly circular; therefore, the resulting entrance areas were slightly less than would be calculated for the above diameters.

For each time series, e-folding times of filling, $\tau$ (in seconds), were calculated as a function of time by

$$[6] \qquad \tau(t) = -\frac{t_2 - t_1}{\ln\left(\frac{c_2 - 1}{c_1 - 1}\right)}$$

where the values of unity in the denominator are the fractional concentration of tracer outside of the cylinder (1 kg/kg). Time constants were calculated at each 0.1 s time step as a 1 s centered moving average.

**Field experiments: a cylindrical cavity exposed to smoke from a small fire**

A schematic diagram of the field experiment is shown in Fig. 1. Sections of thick cardboard (building-form) tubing were used to fashion circular, 30 cm high inner and outer cylinders (inner diameters = 18.5 cm and 29 cm, respectively) of the artificial cavity. The sections were connected by a 9 cm long section of PVC pipe, hereafter referred to as the "tunnel," with an inner diameter of 4 cm. The tunnel was sealed by rubber gaskets and silicone caulk at its intersection with the cylinder. The bottom of the inner cylinder was sealed by a section of aluminum-coated fiberglass. For observation purposes, the top of the inner cylinder was covered by a cap of Pyrex glass sealed around its circumference by silicone caulk. The inner and outer cylinders rested on a flat wooden platform, slightly larger than the outer cylinder, affixed to a small ladder so that the tunnel entrance was 1.4 m above the ground.

CO sensor units were placed at the bottom of the inner cylinder and at the top of the outer cylinder on the tunnel entrance side (Fig. 1). The units were built from CiTicel typel 3F/F carbon monoxide sensors (City Technology Ltd., Portsmouth, UK) on customized circuit boards (courtesy of Robert Kremens, Rochester Institute of Technology) enclosed in 3.3 × 9.3 × 11.8 cm steel boxes with circular inlet openings 2 cm in diameter. The sensors have a nominal range of 0 to 4000 ppm with a maximum limit of 20 000 ppm. The inner CO unit was placed so that its inlet was centered 4 cm above the cylinder floor, and the top unit was positioned so that the center of its inlet was 12 cm directly above the center of the tunnel entrance (Fig. 1). A fine-bead thermocouple (bead diameter = 0.5 mm) was placed at the outer pipe entrance with

**Table 2.** Summary of cavity dimensions and flow and air temperature conditions of the numerical experiments.

| Case | Entrance diameter (cm) | Cavity volume (L) | Wind speed ($m \cdot s^{-1}$) | AOI (°) | $\Delta t$ (°C) |
|---|---|---|---|---|---|
| **Suite 1** | | | | | |
| 1 | 5 | 2.58 | 0–5 | 0 | 0 |
| 2 | 6 | 2.58 | 0–5 | 0 | 0 |
| 3 | 7 | 2.58 | 0–5 | 0 | 0 |
| 4 | 8 | 2.58 | 0–5 | 0 | 0 |
| 5 | 9 | 2.58 | 0–5 | 0 | 0 |
| 6 | 10 | 2.58 | 0–5 | 0 | 0 |
| 7 | 5 | 2.02 | 0–5 | 0 | 0 |
| 8 | 6 | 2.02 | 0–5 | 0 | 0 |
| 9 | 7 | 2.02 | 0–5 | 0 | 0 |
| 10 | 8 | 2.02 | 0–5 | 0 | 0 |
| 11 | 9 | 2.02 | 0–5 | 0 | 0 |
| 12 | 10 | 2.02 | 0–5 | 0 | 0 |
| **Suite 2** | | | | | |
| 13 | 5 | 2.58 | 1.5 | 0 | 0–200 |
| 14 | 6 | 2.58 | 1.5 | 0 | 0–200 |
| 15 | 7 | 2.58 | 1.5 | 0 | 0–200 |
| 16 | 8 | 2.58 | 1.5 | 0 | 0–200 |
| 17 | 9 | 2.58 | 1.5 | 0 | 0–200 |
| 18 | 10 | 2.58 | 1.5 | 0 | 0–200 |
| **Suite 3** | | | | | |
| 19 | 5 | 2.58 | 2 | 0 | 0 |
| 20 | 5 | 2.58 | 2 | 30 | 0 |
| 21 | 5 | 2.58 | 2 | 45 | 0 |
| 22 | 5 | 2.58 | 2 | 60 | 0 |
| 23 | 5 | 2.58 | 2 | 90 | 0 |
| 24 | 7 | 2.58 | 2 | 0 | 0 |
| 25 | 7 | 2.58 | 2 | 30 | 0 |
| 26 | 7 | 2.58 | 2 | 45 | 0 |
| 27 | 7 | 2.58 | 2 | 60 | 0 |
| 28 | 7 | 2.58 | 2 | 90 | 0 |
| 29 | 9 | 2.58 | 2 | 0 | 0 |
| 30 | 9 | 2.58 | 2 | 30 | 0 |
| 31 | 9 | 2.58 | 2 | 45 | 0 |
| 32 | 9 | 2.58 | 2 | 60 | 0 |
| 33 | 9 | 2.58 | 2 | 90 | 0 |

the bead about 1 cm below the center of the tunnel entrance. Three thermocouples of the same type were placed in the inner cylinder so that their beads were centered at heights of 10, 15, and 21 cm above the cylinder floor.

Sonic anemometers (model 81000; R.M. Young Company, Traverse City, Michigan) were placed near the cylinder (Fig. 1) at heights of 2.05 m and 3.1 m aboveground. Wind speeds were averaged over the first and last half hour of the experiment, and the measurements at two heights were fitted to the following power-law relationship:

$$[7] \qquad \frac{U}{U|_{2\,\mathrm{m}}} = \left(\frac{h}{2}\right)^{0.33}$$

where the denominator is the wind velocity at 2 m above the ground. This relationship was used to extrapolate the wind speeds measured at the sonic anemometers to the height of the cavity entrance (1.4 m). Data from the thermocouples and sonic anemometers were logged at 0.1 s intervals by a micrologger (model CR1000; Campbell Scientific, Logan, Utah). Five second moving averages of the wind speed component normal to the cylinder entrance plane were used in the model calculations described below, with negative values (i.e., winds coming from the back side of the cylinder) taken to be zero. AOI was calculated from the vertical and entrance-directed components of wind speed and were also averaged over 5 s intervals. CO concentrations were logged at 5 s intervals.

Woodland fuels (maple twigs, branches, and dry leaf litter) were ignited in a 60 cm diameter fire pit. The center of the pit was positioned 1.2 m in front of the entrance side of the cylinder (Fig. 1). The maximum aboveground height of the fuel was about 30 cm. Fuel was fed to the fire continually for about 1.5 h so that flame heights of 20 to 40 cm were maintained. Although wind direction was erratic, smoke was usually carried toward the cylinder.

**Fig. 2.** Normalized e-folding times plotted against wind speed. The thick solid line marks the empirical relationship $\tau = 0.4/U$.

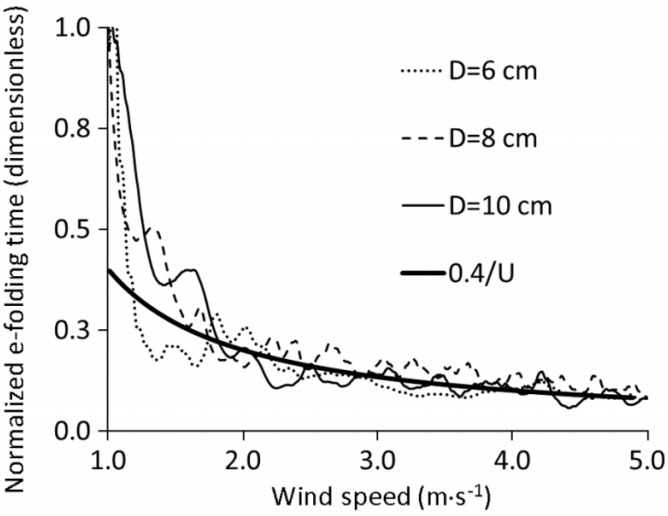


## Results

### Numerical experiments

#### *Wind speed*

Of the three environmental variables, wind speed had the greatest effect on the e-folding times of filling for a given entrance diameter, with e-folding times proportional to $1/U$ (Fig. 2). Figure 3 displays the empirically estimated coefficients of e-folding times ($k$ in eq. 4) for the cavities with 2.58 L and 2.02 L volumes plotted against the volume to entrance area ratio ($V/A$) of the simulated cavities. The resulting regression equation

$$[8] \qquad k = 102.3\frac{V}{A} - 22.6 \quad (R^2 = 0.94,\ \mathrm{SE} = 11.3,\ n = 12)$$

provided the coefficient for eq. 4 and was used in the model as described below (eqs. 10–11).

**Fig. 3.** Coefficients of e-folding times ($k$, in metres; eq. 8) correlated with the volume to entrance area ratio ($V/A$) of the cavities. The triangle represents the physical experiment. Note the broken $x$ and $y$ axes.

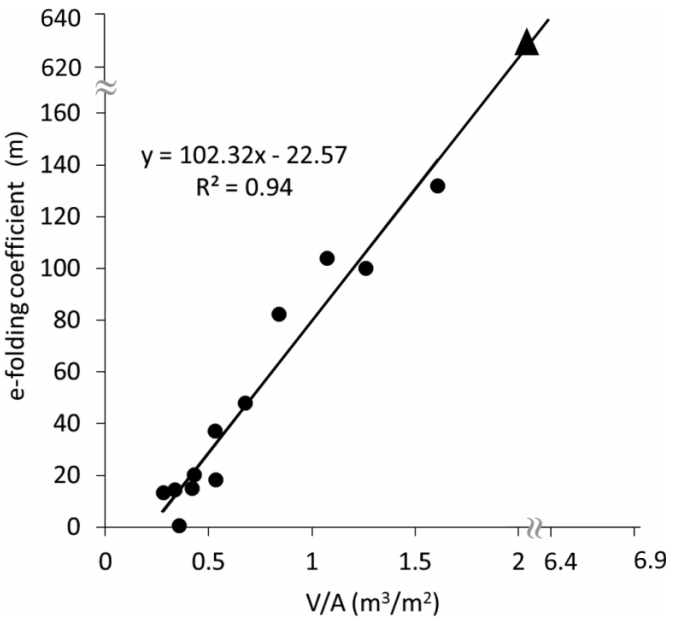


### *Temperature*

In the experiments with variable temperatures between the inside and outside of the cavity, temperature gradients between the top and bottom of the cavities were generally large, with heated gas buoyed to the top (Fig. 4). In all of the simulations, temperatures near the floor of the cavity remained near their original temperature (20 °C), whereas maximum temperatures at the midheight in the cavity remained less than or equal to about 60 °C.

For all simulations, e-folding times rose with outside gas temperature and stayed elevated even as temperatures within the entrance tunnel approached the maximum outside temperature (220 °C). This suggests that the external gas temperature itself, rather than the temperature difference between the inside and outside of the cavity, is responsible for this effect.

### *Angle of incidence (AOI)*

Figure 5 indicates the time constants of filling for entrance tunnel diameters of 5, 7, and 9 cm over the range of tested angles. Clearly, AOI has the greatest effect at the smallest diameter, and the effect decreases with increasing entrance diameter. In all cases, the inward volume flux decreases as AOI approaches 45° and increases back to its approximate value at AOI = 0°. This occurs because the dynamic pressure at the entrance decreases as AOI increases toward 45° and then the static pressure decreases as flow becomes more parallel to the entrance plane. A general empirical equation can be derived by normalizing the data for each entrance diameter by the e-folding time at AOI = 0, which is the maximum or near-maximum e-folding time for each diameter. The fitted polynomial gives a dimensionless multiplication factor, $f(\mathrm{AOI})$, which modifies the zero-angle e-folding times:

$$[9] \quad f(\mathrm{AOI}) = 2 \times 10^{-4}\mathrm{AOI}^2 - 2 \times 10^{-2}\mathrm{AOI} + 1 \qquad (R^2 = 0.83,\ n = 15)$$

### Field experiment

Fire-induced, above-ambient CO levels were relatively low (<80 ppm above ambient) throughout the experiment, whereas inside-cavity levels remained below 30 ppm above ambient (Fig. 6). Although temperatures recorded by the thermocouple at the outer side of the entrance reached as high as 60 °C, temperatures inside the cylinder fluctuated by only about 1 °C from their initial temperature (34 °C) (Fig. 6). The temperature gradient between the top and bottom internal thermocouples was correspondingly low, averaging only 2.6 °C·m$^{-1}$.

### Evaluation of the model: comparing the numerical and field experiments

For air quality and species conservation purposes, it is desirable that a model of combustion product levels errs toward overestimates rather than underestimates. Thus, we simplified the model by omitting the effects of temperature, thereby keeping the e-folding times at a minimum. The general empirical model for e-folding times of single-entrance in-cavity combustion product concentrations is

$$[10] \quad \tau(U_t, \mathrm{API}_t) = f(\mathrm{AOI}_t)\frac{k}{U_t}$$

where $U_t$ and $\mathrm{AOI}_t$ are the mean wind speed and AOI, respectively, at time $t$, $f(\mathrm{AOI}_t)$ is calculated from $\mathrm{AOI}_t$ using eq. 9, and $k$ is calculated from eq. 8. Substituting the terms derived in those equations, we obtain the complete formulation:

$$[11] \quad \tau(U_t, \mathrm{AOI}_t) = 2 \times 10^{-4}\mathrm{AOI}^2 - 2 \times 10^{-2}\mathrm{AOI} + 1 \times \frac{102.3\frac{V}{A} - 22.6}{U_t}$$

In the field experiment, the ratio of cavity volume to entrance area of the cylinder was 6.37 m$^3$·m$^{-2}$, giving $k$ = 629 m (eq. 8). Wind speeds were measured by sonic anemometers, and e-folding times were estimated for each time step by eq. 11. Using these e-folding times, in-cavity CO concentration was estimated at each time step by eq. 5.

Figure 7 shows the outside and in-cavity gas temperatures and CO concentrations measured during the experiment. In Fig. 8, results of the model are superimposed on the measurements of in-cavity CO. In the linear regression used to generate the formula for the coefficient $k$ (eq. 8), the 95% confidence interval for the coefficient of $V/A$ ranged from 84.2 to 120.4, and the intercept ranged from –37.1 to –8.0. These values were substituted into eq. 8 to create a range of model estimates indicated by the broken lines in the main plot and the inset. Although missing the extremes, the model closely follows the mean of in-cavity CO, with a standard error of only 3 ppm, whereas the estimated CO dose (Fig. 8, inset) matches the measured dose almost perfectly, with a standard error of only 1 ppm·h. Interestingly, using a constant angle of about 30° (where $f(\mathrm{AOI})$ = 0.6) gave nearly the same result as using the AOI calculated at each time step (not shown).

**Fig. 4.** The e-folding times for cylinders with entrances of 6 and 10 cm in diameter plotted against the external gas temperature.

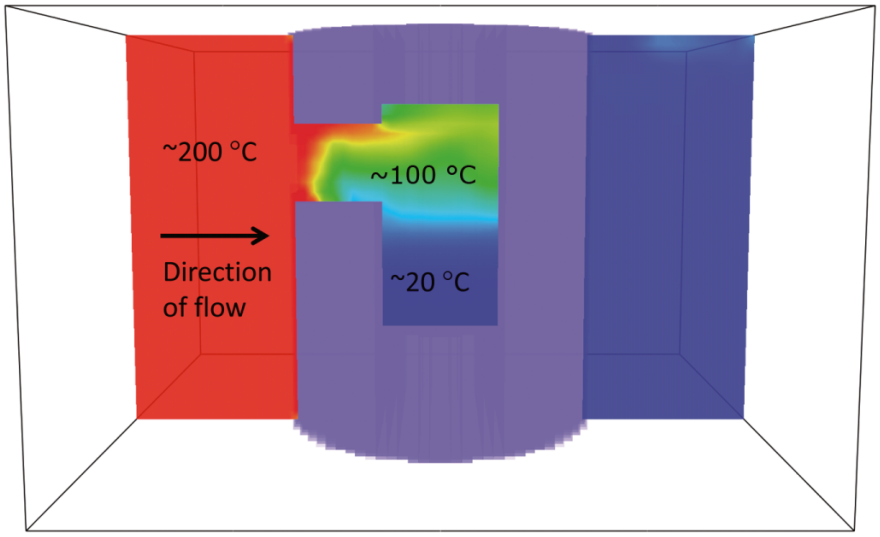


**Fig. 5.** The effect of angle of incidence (AOI) on e-folding times for cylinders with entrances of 5, 7, and 9 cm in diameter.

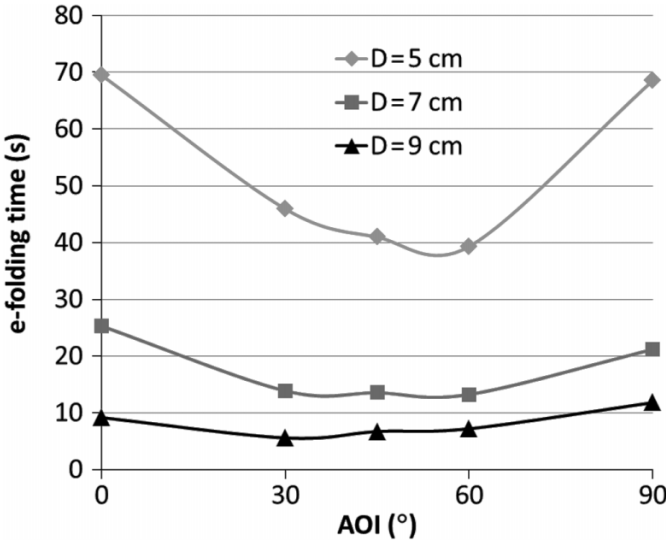


**Fig. 6.** The same data as in Fig. 5, with e-folding times normalized by the values at AOI = 0°, the maximum or near-maximum value for each series.

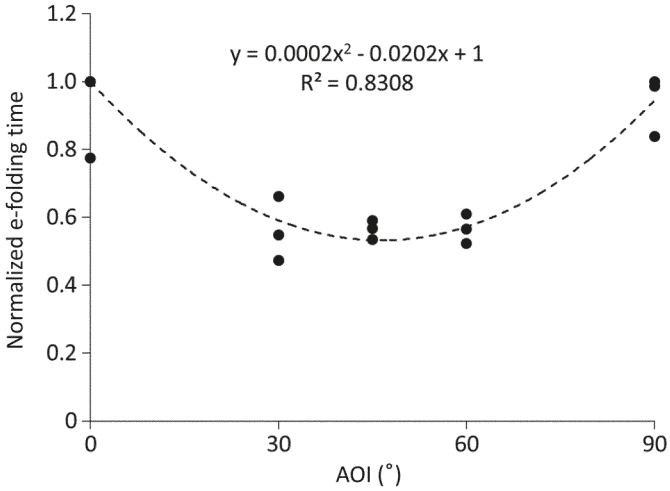


### *Practical application of the model*

Detailed time series of combustion product concentrations and wind speeds near a cavity will obviously not be available to forest managers who wish to quickly estimate or forecast future wildland fire impacts on sheltered fauna. However, concentrations of various gases and gas temperatures above a wildland fire may be, with some simplification, characterized by a lognormal function, originally used to model temperature curves in compartment fires. This "source function" is of the form

$$[12] \qquad \varphi(t) = a \exp\left[\frac{\left(\ln(t) - \ln(t_{\max})\right)^2}{s}\right]$$

where $\varphi$ is the concentration of an arbitrary ignition product, and the amplitude ($a$), time of maximum ($t_{max}$), and shape factor ($s$) are fitted empirically (Barnett 2002). In addition, a single, mean wind speed is sufficient for the model represented by eq. 11, relieving the need for detailed measurements.

As an example, we applied eq. 11 using cavity dimensions typical of the red-cockaded woodpecker (RCW) (*Picoides borealis* Vieillot, 1809), an endangered species (Driver et al. 2002). For realism, we also used measured CO concentrations and horizontal wind velocities at a height of 6.1 m at 10 s intervals during a prescribed, experimental surface fire (Dickinson et al. 2010). The height at which the CO measurements were taken is within the typical nesting height range of a wide variety of North American woodpeckers (Scott et al. 1977). A typical volume of a RCW cavity is 2.2 L, with an entrance that is somewhat oblong vertically,

**Fig. 7.** Data from the field experiment. CO concentration (above ambient) outside the cylinder (thick black line) and in the cavity (thick gray

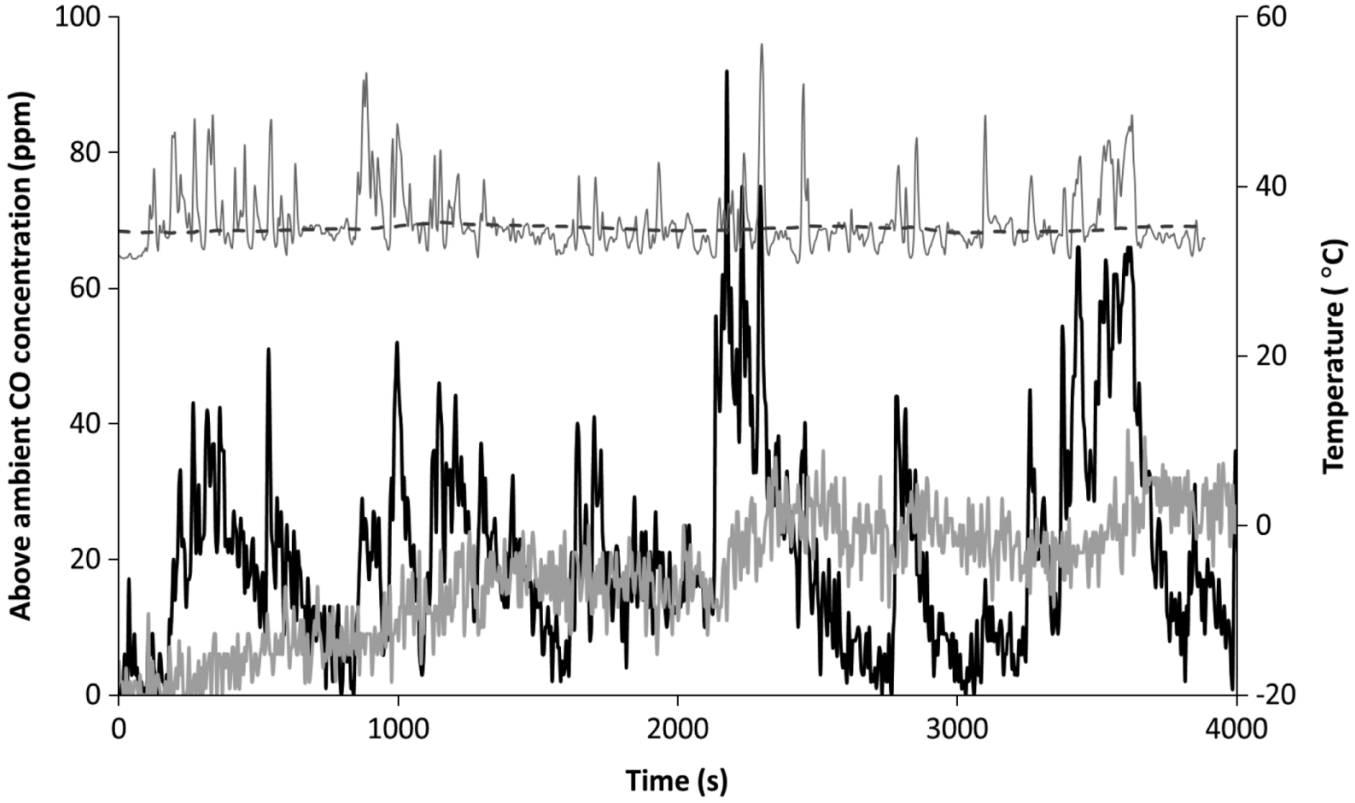


**Fig. 8.** Measured in-cavity CO concentration (jagged gray line) and modeled concentration (solid black line). The broken lines indicate the

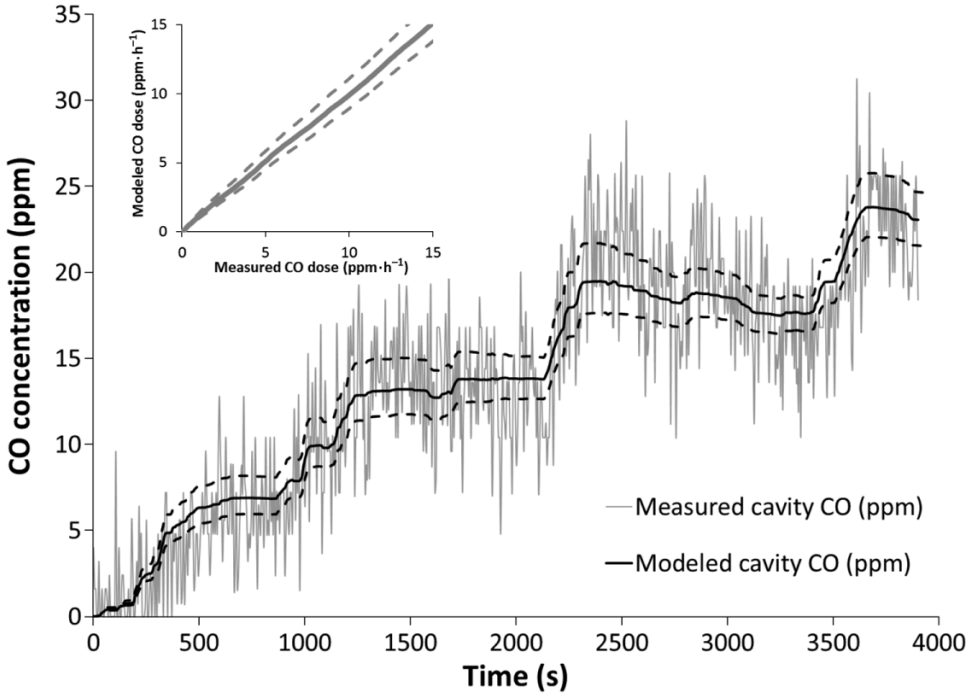

**Fig. 9.** Example application of the model to a cavity typical of the red-cockaded woodpecker. Thin gray line: outside CO concentrations measured during a prescribed surface fire. Black line: model estimate of in-cavity CO, calculated from the observed, high-frequency time series of outside CO and wind speed. Broken thick gray line: outside CO concentration, calculated from lognormal curve fitted to the CO measurements. Thick gray line: model estimate of cavity CO from the lognormal curve and a single, mean wind speed (0.68 $m \cdot s^{-1}$). Inset: the same, but for accumulated CO dose.

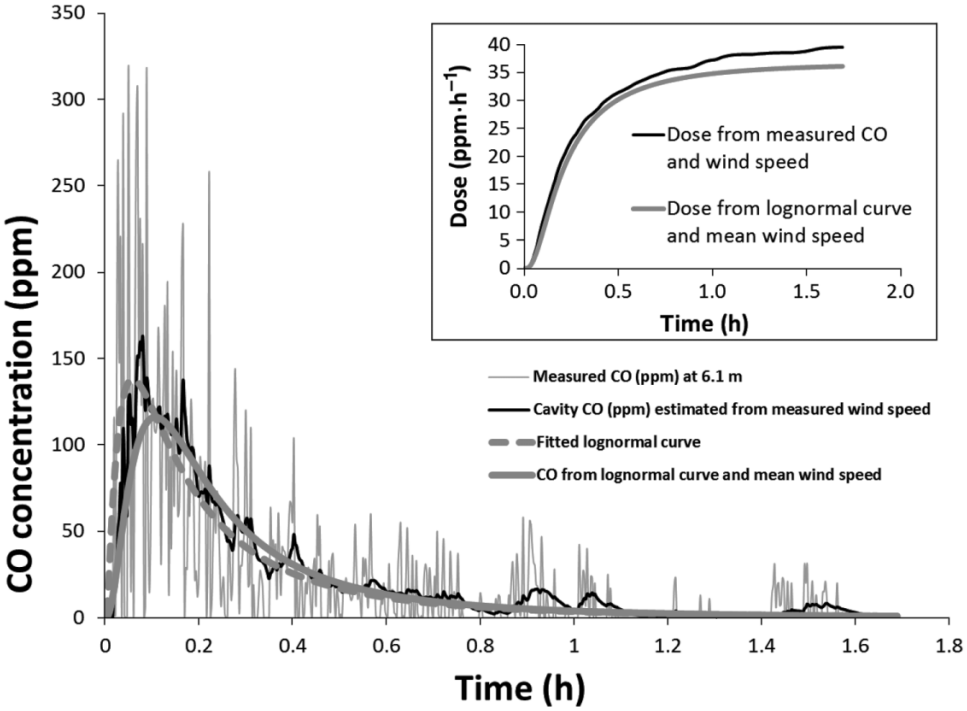


but with an effective diameter of about 5 cm (Driver et al. 2002). This gives it a relatively low *V*/*A* of 1.12 $m^3 \cdot m^{-2}$ and, from eq. 8, an e-folding coefficient of about 90 m. In this example, AOI was taken to be zero.

Figure 9 contains a time series of the measured CO concentrations (thin gray line) outside the cavity, as well as estimated CO concentration (broken thick gray line) calculated using eq. 11. We determined the parameters of the source function (eq. 12) (maximum amplitude = 137.9 ppm; time of maximum = 213 s; shape constant = 2.17) using a least squares fit parameterization of the CO measurements.

The in-cavity CO levels estimated by our model using eq. 5, with the estimated source function (eq. 12) used as the outside CO concentration, $c_\infty$, and the overall mean wind speed (thick gray line) used as a constant wind speed, match remarkably well with those represented by the curve calculated from measured CO levels outside the cavity and 10 Hz variable wind speeds (black line), suggesting that in-cavity CO concentrations are not sensitive to rapid fluctuations in wind speed and external CO concentration. Therefore, this method of estimation can provide robust forecasts even without high-frequency data (Fig. 9). The time series of resulting estimated doses (i.e., the product of concentration and time) obtained from the mean wind speed and lognormal curve also compares well with that calculated from the measured time series of observed wind and CO concentrations (Fig. 9, inset). Note that at no point throughout this low-intensity fire event did the concentrations reach a level that would be considered harmful to cavity occupants.

## Discussion

The close correspondence between measured and modeled CO levels in the physical cavity (Fig. 8) would be notable even if it resulted from a direct simulation of the fabricated cavity. What makes the match more remarkable and useful is that it was the result of a simplified equation derived from numerical experiments involving cavities of dimensions significantly different from the experimental cavity, resulting in differing cavity *V*/*A* (Table 3). Furthermore, the model seems to provide reasonable estimates without the need for high-frequency wind and external concentration data (Fig. 9). As with all such models, further evaluation regarding margins of error and performance in different environments and shelter types than were explored here are required. However, the results above suggest that numerical experiments are a useful and productive approach to obtaining models of wildland fire effects. In addition, they provide considerable savings of cost and time over comparable field experiments.

The tracer gas in the simulations was treated as an ideal gas and a conserved scalar (i.e., it was of neutral buoyancy, did react chemically to evolve into other gas species, and was not adsorbed by the cavity inner or outer walls); therefore, the model may not apply to products such as soot, which are not neutrally buoyant, or to highly reactive or vegetation-adsorbed species over a long term. By treating gas temperature as a combustion product, it is possible that eq. 5 could be used to estimate increased gas temperatures in the cavity, another potential harmful effect of fire, with the caveats that the estimated internal temperature applies to the tunnel and

**Table 3.** Cavity volume to entrance area ratios (*V/A*) calculated from experimental studies of gas mixing and for natural and artificial cavities.

| Source | Region | Study details | Description | *V/A* (m) |
|---|---|---|---|---|
| **Gas-mixing studies** | | | | |
| This study | NA | Cavities with circular entrances and cylindrical interior volumes | Minimum *V/A* in numerical experiments | 0.3 |
| | | | Maximum *V/A* in numerical experiments | 1.6 |
| | | | Experimental cavity | 6.4 |
| Ar et al. 2004 | Middle East | Circular entrance and cylindrical cavity | Experimental Syrian woodpecker (*Dendrocopos syriacus*) cavity | 1.4 |
| **Natural cavities** | | | | |
| Ligon 1970 | North America | Southeastern US pine savanna, cavity information is from Ligon (1970) except for cavity diameter, which was from Copeyon et al. (1991), elliptical entrances and cylindrical cavities assumed | Red-cockaded woodpecker (*Picoides borealis*) | 0.4 |
| Aubrey and Raley 2002 | North America | US Pacific Northwest, elliptical entrances and cylindrical cavities assumed | Pileated woodpecker (*Dryocopus pileatus*) | 1.1 |
| | | | Northern flicker (*Colaptes auratus*) | 0.4 |
| | | | Lewis' woodpecker (*Melanerpes lewis*)[a,b] | 7.1 |
| | | | White-headed woodpecker (*Picoides albolarvatus*)[a,b] | 2.0 |
| | | | Acorn woodpecker (*Melanerpes formicivorus*)[b] | 5.2 |
| | | | Williamson's sapsucker (*Sphyrapicus thyroideus*)[a,b] | 1.1 |
| | | | Red-naped sapsucker (*Sphyrapicus nuchalis*) | 2.1 |
| Murphy et al. 2003 | Australia | Savanna woodland, Cape York Peninsula, Australia, elliptical entrances and cylindrical cavities assumed | Palm cockatoos (*Probosciger aterrimus*)[a,b,c] | 1.1 |
| Saunders et al. 1982 | Australia | Eucalyptus woodland, southwestern Australia, elliptical entrances and cylindrical cavities assumed | Red-tailed black cockatoos (*Calyptorhynchus magnificus*) | 2.1 |
| | | | Corellas (*Cacatua pastinator*) | 2.0 |
| | | | Galahs (*Cacatua roseicapilla*) | 1.4 |
| | | | Port Lincoln parrots (*Barnadius zonarius*) | 0.7 |
| Haseler and Taylor 1993 | Australia | Eucalyptus forest, Tasmania, elliptical entrances and cylindrical cavities assumed | Green rosella (*Platycercus caledonicus*), branch hollow | 0.5 |
| | | | Green rosella (*Platycercus caledonicus*), pipe hollow | 1.5 |
| | | | Green rosella (*Platycercus caledonicus*), other trunk hollow | 12.3 |
| Ar et al. 2004 | Middle East | Israel, elliptical entrances and cylindrical cavities assumed | Syrian woodpecker (*Dendrocopos syriacus*) | 1.2 |
| **Artificial cavities and boxes** | | | | |
| Taylor and Hooper 1991 | North America | Drilled cavities in live trees, circular entrance and cylindrical cavity | Red-cockaded woodpecker (*Picoides borealis*), drilled cavity | 0.4 |
| Menkhorst 1984 | Australia | Nest boxes with circular entrances and cubical cavities, ordered by *V/A* | Bird and marsupial nest box, 15 cm entrance diameter | 1.7 |
| | | | Bird and marsupial nest box, 12 cm entrance diameter | 2.7 |
| | | | Bird and marsupial nest box, 8 cm entrance diameter | 6.1 |
| | | | Bird and marsupial nest box, 5 cm entrance diameter | 15.6 |
| Wardell-Johnson 1986 | Australia | Nest boxes with elliptical and circular entrances and cubical cavities, boxes numbered in accordance to source and ordered by *V/A* | Mardo (*Antechinus flavipes leucogaster*), nest box type 7 | 0.7 |
| | | | Mardo (*Antechinus flavipes leucogaster*), nest box type 6 | 1.4 |
| | | | Mardo (*Antechinus flavipes leucogaster*), nest box type 8 | 4.8 |
| | | | Mardo (*Antechinus flavipes leucogaster*), nest box type 5 | 4.6 |
| | | | Mardo (*Antechinus flavipes leucogaster*), nest box type 2 | 5.1 |
| | | | Mardo (*Antechinus flavipes leucogaster*), nest box type 3 | 6.1 |
| | | | Mardo (*Antechinus flavipes leucogaster*), nest box type 1 | 6.2 |
| | | | Mardo (*Antechinus flavipes leucogaster*), nest box type 4 | 7.5 |
| Lindenmayer et al. 2009 | Australia | Nest boxes with circular entrances and cubical cavities | Small marsupial nest box | 9.3 |
| | | | Large marsupial nest box | 4.6 |

**Note:** Cavity configurations are restricted, where verification was possible, to cavities in which the single entrance was near the top of the interior volume. Many studies did not provide enough information from which to estimate configurations and volumes and could not be included in this table. Higher *V/A* values result in reduced mixing rates.

[a]Diameter at the midpoint of the range.

[b]Volume at the midpoint of the range.

[c]Active nests; 42% were enclosed cavities resulting from branch drop, the rest were open-top cavities from trunk shear.

uppermost regions of the cavity and that temperature gradients are likely to be large (and not predictable by the simplified model) as temperature increases. Applying eq. 5 to the measured external temperatures in the field experiment gives an estimated increase of about 3 °C in the cavity, which is only a slight overprediction of the actual maximum temperature observed at the top of the cavity.

The effect of temperature differences between the outside

and inside of the cavity on e-folding times is most likely the result of the lower density of the heated gas. Depending on the entrance diameter, gas volume fluxes either stayed roughly constant or increased by as much as 100%, though oscillating rapidly and sometimes erratically, as the outside gas temperature rose. However, density of an ideal gas is inversely proportional to temperature, so the density of the tracer gas decreased to about 62% of its room temperature value over the course of the simulation, thereby decreasing mass flux (the product of density and volume flux) enough to compensate, or overcompensate, for the increased volume flux and increase e-folding times of filling overall.

It is unlikely that a buoyant plume within a forest canopy would maintain a constant direction directly toward a real cavity entrance (i.e., it is just as likely to approach the side of the bole opposite the canopy entrance). In addition, the plume will "puff" and also be influenced by the local, and most likely turbulent, wind field. Therefore, because the model represented by eq. 10 assumes a constant flow direction toward the cavity entrance, it may significantly overpredict cavity concentrations in a real wildland fire scenario. As with other engineering risk analysis models, this is desirable because the model then provides a built-in safety factor. Though our example model application (Fig. 9) assumed a constant AOI of 0°, in future applications, it would be more conservative to assume an AOI of 45° because it results in reduced e-folding times and, thus, more rapid mixing. Note also that no allowance has been made for the effect that occupants of the cavity might have, either by respiration or by convective flow from body heat, on the ventilation rate.

Equation 5, in combination with the observed mean wind speed and eqs. 11 and 12, which provide empirical approximation for the values of the parameters needed by eq. 5, may have wide applicability as the range of cavity *V*/*A* spanned by the numerical and physical experiments overlaps a variety of single-entrance tree cavities found around the world, both natural and artificial (Table 3). However, eq. 5 most likely does not apply to single-entrance burrows or, because of chimney effect, shelters with multiple entrances at different heights (e.g., hollowed tree boles with entrances both near their bases and well above the ground). In addition, the effects of entrance tunnel length and stem diameter were not studied, though their impacts on the model are expected to be minimal. Shelters for which the entry tunnel is at the midpoint or bottom of the cavity may not have the same response as the top-tunnel cavities used in these experiments, because heated gases may be trapped at the top of the cavity. Further work on the model should include the incorporation of toxicity effects and the use of standard lognormal curves to approximate the concentrations of toxins outside the shelter (eq. 12), based on fire plume simulations, to represent time series of gas concentrations and temperatures at various heights over a range of fire spread rates and intensities. In addition, the interaction between forest canopy structure and wind can modify the turbulence statistics (Bohrer et al. 2009) and resulting dispersion within the canopy subdomain (Bohrer et al. 2008) and therefore affect aeration rates in single-entrance cavities. Thus, the effect of the forest canopy on gas flow should ultimately be included. Finally, buoyant flow caused by the body heat of cavity occupants may be added to the model to ensure realistic modeling of cavity ventilations rates.

## Conclusion

The correspondence between modeled levels of cavity CO and those measured in the field experiment is encouraging and supports the concept of model building by virtual experiments. The model represented by eqs. 5, 11, and 12 provides a useful tool for estimating the concentration of combustion products in a single-entrance cavity exposed to wildland fire (Fig. 9). To the authors' knowledge, such a tool has been heretofore unavailable. As is the usual practice in engineering and fire management, the model tends toward overestimates, thus providing a safety factor for forest managers and ecologists who wish to estimate, based on burn prescriptions and meteorological predictions, the possible effects of wildland fire on sheltered fauna.

## Acknowledgements

We thank William (Ruddy) Mell, Randy McDermott, and Kevin McGrattan for their suggestions during this project and Kyle Maurer and Dekel Shlomo for assistance in the fire experiment. We also thank Robert Kremens, who designed and built the meteorology and CO sensor packages used to obtain the data shown in Figs. 7, 8, and 9. This work was supported by a grant from the Joint Fire Sciences Program (05-2-1-24) and the National Fire Plan. A.B. was funded in part by NASA-NESSF (fellowship NNX09A026H). G.B. was funded in part by the U.S. Department of Agriculture (USDA) Forest Service Northern Research Station Laboratory in Lansing, Michigan (research joint venture agreement FS-NRS-06-Fire-10-01), the USDA Forest Service Northern Research Station in Delaware, Ohio (agreement 09-CR-11242302-033), the U.S. Department of Energy's Office of Science (BER) through the Midwestern Regional Center of the National Institute for Climatic Change Research at Michigan Technological University (award DE-FC02-06ER64158), and the National Science Foundation (grants DEB-0911461 and DEB-0918869). Any opinions, findings, and conclusions or recommendations expressed in this material are those of the author(s) and do not necessarily reflect the views of the National Science Foundation.

## References

Ar, A., Barnea, A., Yom-Tov, Y., and Mersten-Katz, C. 2004. Woodpecker cavity aeration: a predictive model. Respir. Physiol. Neurobiol. **144**(2–3): 237–249. doi:10.1016/j.resp.2004.04.019. PMID:15556106.

Aubrey, K.B., and Raley, C.M. 2002. The pileated woodpecker as a keystone habitat modifier in the Pacific Northwest. *In* Proceedings of the Symposium on the Ecology and Management of Dead Wood in Western Forests. *Edited by* W.F. Laudenslayer, P.J. Shea, B.E. Valentine, C.P. Weatherspoon, and T.E. Lisle. USDA Forest Service, Pacific Southwest Research Station, General Technical Report PSW-GTR-181. pp. 257–274.

Barnett, C.R. 2002. BFD curve: a new empirical model for fire compartment temperatures. Fire Saf. J. **37**(5): 437–463. doi:10.1016/S0379-7112(02)00006-1.

Bohrer, G., Katul, G.G., Nathan, R., Walko, R.L., and Avissar, R. 2008. Effects of canopy heterogeneity, seed abscission and inertia

on wind driven dispersal kernels of tree seeds. J. Ecol. **96**(4): 569–580. doi:10.1111/j.1365-2745.2008.01368.x.

Bohrer, G., Katul, G.G., Walko, R.L., and Avissar, R. 2009. Exploring the effects of microscale structural heterogeneity of forest canopies using large-eddy simulations. Boundary-Layer Meteorol. **132**(3): 351–382. doi:10.1007/s10546-009-9404-4.

Chaplin, G.C., Randall, J.R., and Baker, C.J. 2000. The turbulent ventilation of a single opening enclosure. J. Wind Eng. Ind. Aerodyn. **85**(2): 145–161. doi:10.1016/S0167-6105(99)00136-1.

Copeyon, C.K., Walters, J.R., and Carter, J.H., III. 1991. Induction of red-cockaded woodpecker group formation by artificial cavity construction. J. Wildl. Manage. **55**(4): 549–555. doi:10.2307/3809497.

Dickinson, M.B., Norris, J., Bova, A.S., Kremens, R.L., Young, V., and Lacki, M.J. 2010. Effects of wildland fire smoke on a tree-roosting bat: integrating a plume model, field measurements, and mammalian dose–response relationships. Can. J. For. Res. **40**(11): 2187–2203. doi:10.1139/X10-148.

Driver, C., Ollero, J., Su, Y.F., Fulton, R., Dennis, G., Tiller, B., Balbach, H., and Reinbold, K. 2002. Effects of fog oil smoke on the hatchability and fledgling survival of the house sparrow (*Passer domesticus*), a nestling-surrogate for the red-cockaded woodpecker. U.S. Army Corps of Engineers, Engineer Research and Development Center, ERDC/CERL Technical Report TR-02-34.

Engstrom, R.T. 2010. First-order fire effects on animals: review and recommendations. Fire Ecol. **6**(1): 115–130. doi:10.4996/fireecology.0601115.

Etheridge, D.W. 2002. Nondimensional methods for natural ventilation design. Build. Environ. **37**(11): 1057–1072. doi:10.1016/S0360-1323(01)00091-9.

Franzreb, K.E. 1997. Success of intensive management of a critically imperiled population of red-cockaded woodpeckers in South Carolina. J. Field Ornithol. **68**(3): 458–470.

Guelta, M., and Balbach, H.E. 2005. Modeling fog oil obscurant smoke smoke penetration into simulated tortoise burrows and bat colony trees. U.S. Army Corps of Engineers, Engineer Research and Development Center, ERDC/CERL Technical Report TR-05-31.

Guelta, M., and Checkai, R.T. 2001. Methodology for measurement of fog oil smoke penetration into a red-cockaded woodpecker nest cavity. U.S. Army Soldier and Biological Chemical Command, Edgewood Chemical Biological Center, ECBC-TR 152.

Haseler, M., and Taylor, R. 1993. Use of tree hollows by birds in sclerophyll forest in north-eastern Tasmania. Tasforests, **4**: 51–56.

Ligon, J.D. 1970. Behavior and breeding biology of the red-cockaded woodpecker. Auk, **87**: 255–278.

Lindenmayer, D.B., Welsh, A., Donnelly, C., Crane, M., Michael, D., Macgregor, C., McBurney, L., Montague-Drake, R., and Gibbons, P. 2009. Are nest boxes a viable alternative source of cavities for hollow-dependent animals? Long-term monitoring of nest box occupancy, pest use and attrition. Biol. Conserv. **142**(1): 33–42. doi:10.1016/j.biocon.2008.09.026.

McGrattan, K., McDermott, R., Prasad, K., Hostikka, S., and Floyd, J. 2009*a*. Fire Dynamics Simulator (FDS) (version 5). FDS technical reference guide. Volume 3: validation. NIST Special Publ. 1018-5. Available at http://www.fire.nist.gov/fds/documentation.html (accessed on 4 February 2010).

McGrattan, K., Hostikka, S., and Floyd, J. 2009*b*. Fire Dynamics Simulator (FDS) (version 5). FDS user guide. NIST Special Publ. 1019-5. Available at http://www.fire.nist.gov/fds/documentation.html (accessed 4 February 2010).

Menkhorst, P.W. 1984. Use of nest boxes by forest vertebrates in Gippsland: acceptance, preference, and demand. Aust. Wildl. Res. **11**(2): 255–264. doi:10.1071/WR9840255.

Murphy, S., Legge, S., and Heinsohn, R. 2003. The breeding biology of palm cockatoos (*Probosciger aterrimus*): a case of a slow life history. J. Zool. (Lond.), **261**(4): 327–339. doi:10.1017/S0952836903004175.

O'Brien, J.J., Stahala, C., Mori, G.P., Callaham, M.A., Jr., and Bergh, C.M. 2006. Effects of prescribed fire on conditions inside a Cuban Parrot (*Amazona leucocephala*) surrogate nesting cavity on Great Abaco, Bahamas. Wilson J. Ornithol. **118**(4): 508–512. doi:10.1676/05-118.1.

Okubo, A., and Levin, S.A. 2001. Diffusion and ecological problems: modern perspectives. 2nd ed. Springer-Verlag, New York.

Saunders, D.A., Smith, G.T., and Rowley, I. 1982. The availability and dimensions of tree hollows that provide nest sites for cockatoos (Psittaciformes) in Western Australia. Aust. Wildl. Res. **9**(3): 541–556. doi:10.1071/WR9820541.

Scott, V.E., Evans, K.E., Patton, D.R., and Stone, C.P. 1977. Cavity-nesting birds of North American forests. USDA Forest Service, Agric. Handb. 511. Available from http://www.na.fs.fed.us/spfo/pubs/wildlife/nesting_birds (accessed 21 January 2010).

Taylor, W.E., and Hooper, R.G. 1991. A modification of Copeyon's drilling technique for making artificial red-cockaded woodpecker cavities. USDA Forest Service, Southeastern Forest Experiment Station, GTR-SE-72.

Wardell-Johnson, G. 1986. Use of nest boxes by mardos, *Antechinus flavipes leucogaster*, in regenerating Karri forest in South Western Australia. Aust. Wildl. Res. **13**(3): 407–417. doi:10.1071/WR9860407.